JOURNAL OF AIRCRAFT
Vol. 31, No. 3, May–June 1994

Chine-Shaped Forebody Effects on Directional Stability at High-α

R. Ravi* and William H. Mason†
Virginia Polytechnic Institute and State University, Blacksburg, Virginia 24061

Computational fluid dynamics has been used to study the flowfields over chine-shaped forebodies at low-speed high angle-of-attack conditions with sideslip. The purpose is to define forebody geometries that provide good directional stability characteristics under these conditions. An analytically defined generic forebody model is described, and a parametric study of various forebody shapes was then conducted to determine which shapes promote a positive contribution to directional stability at high angle of attack. An unconventional way of presenting the results is used to illustrate how the positive contribution arises. The effect of cross-sectional shape on directional stability was found to be very significant. Broad chine-shaped cross sections were found to promote directional stability. Also, directional stability is improved if the chine is placed closer to the top of the cross section. Planform shapes also played an important role in determining the forebody directional stability characteristics. Based on the results of this initial parametric study, some guidelines for aerodynamic design to promote positive directional stability are presented.

Nomenclature

a = maximum half-breadth of the forebody definition
b = maximum centerline of the forebody definition
b' = wingspan based on Erickson's wind-tunnel model, 46.8 in.
C_n = yawing-moment coefficient, yawing moment/$q_\infty S_{\text{ref}} b'$
$C_{n\beta}$ = directional stability derivative, $\partial C_n/\partial\beta$
C_p = pressure coefficient, $(p - p_\infty)/q_\infty$
c_y = sectional side force, section side force/q_∞
d = maximum forebody planform width, 8.7 in.
l = forebody length, 30 in.
M_∞ = freestream Mach number, 0.2
m, n = adjustable parametric coefficients
p = pressure
p_∞ = freestream pressure
q_∞ = freestream dynamic pressure
Re_l = Reynolds number based on model length, 1.02×10^6
S_{ref} = reference area based on Erickson's wind-tunnel model wing area, 1264.32 in.^{2}
u^* = wall friction velocity, $\sqrt{\tau_w/\rho}$
V_{sep} = crossflow velocity magnitude at separation point (chine edge)
x, y, z = coordinate system: x positive aft along model axis, y positive to right, and z positive up
xn = distance from the nose tip to the station where the planform span becomes a constant
y^+ = inner law variable, yu^*/ν
α = angle of attack, deg
β = angle of sideslip, deg
ΔC_p = difference between leeward and windward C_p across the vertical plane of symmetry
ν = kinematic viscosity
ρ = density
τ_w = shear stress at the wall

Presented as Paper 92-0030 at the AIAA 30th Aerospace Sciences Meeting and Exhibit, Reno, NV, Jan. 6–9, 1992; received Aug. 6, 1992; revision received Oct. 31, 1992; accepted for publication Oct. 31, 1992. Copyright © 1994 by the American Institute of Aeronautics and Astronautics, Inc. All rights reserved.

*Graduate Research Assistant, Department of Aerospace and Ocean Engineering. Student Member AIAA.
†Associate Professor, Department of Aerospace and Ocean Engineering. Associate Fellow AIAA.

Introduction

FUTURE advanced fighters are likely to possess chine-type forebodies, as evidenced by the YF-22 and YF-23 configurations (Fig. 1). For these aircraft, high levels of agility are demanded, and the aerodynamic characteristics at high angle of attack play an important role in determining aircraft handling qualities and agility. At high angle of attack, forebody aerodynamic characteristics make significant contributions to the complete configuration aerodynamics.

One specific characteristic of interest is directional stability. For the F-5A, which has good high angle-of-attack characteristics, it has been shown experimentally[1] that the forebody makes a significant positive contribution to directional stability at angles of attack above which the vertical tail ceases

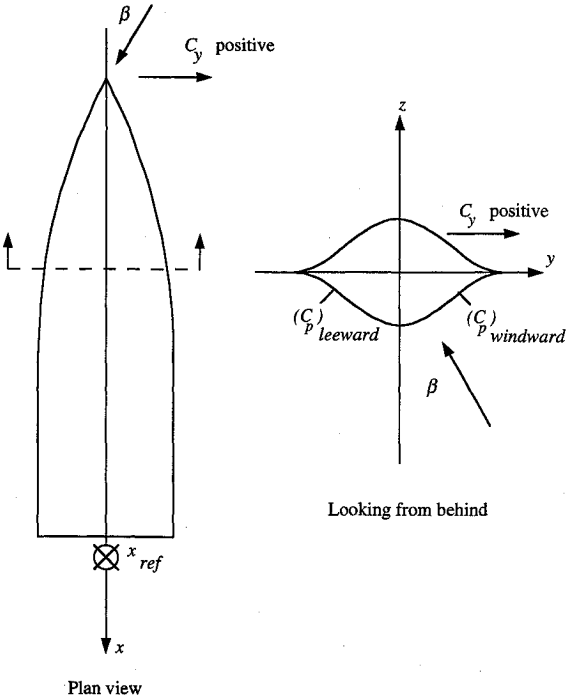

Fig. 1 Sign convention used in the forebody study.

to be effective. The F-5A forebody had a smooth cross section, although it was not axisymmetric. The current authors recently demonstrated that the F-5A experimental results could also be predicted using computational fluid dynamics (CFD) methods.[2] The ability to reproduce previously obtained experimental results meant that it would be valid to use CFD to try to design shapes for specific aerodynamic characteristics at high angle of attack, where large regions of separated flow are present.

In general, current objectives of aerodynamic forebody design require that a stabilizing contribution to directional stability ($C_{n\beta} > 0$) at moderate angles of attack ($\alpha \approx 15$–30 deg) be obtained without producing extreme stability at high angle of attack ($\alpha \approx 40$–60 deg), which is considered to contribute to poor yaw-damping characteristics. Tailoring the aerodynamic properties of forebodies through forebody shaping could greatly improve aircraft performance, and minimize the associated problem of vehicle stabilization and control. The survey by Chambers,[3] and more recently by Rom,[4] define the basis of the current understanding of high angle-of-attack aerodynamics.

Because of the interest in chine-shaped forebodies, a key issue in the application of computational methods to forebody design is the ability to treat chine sectional shapes. Few general chine-shaped forebody wind-tunnel tests are available to use for comparison with computational methods. One is the wind-tunnel investigation conducted by Erickson and Brandon[5] (the "Erickson forebody"). In that test chine effects were investigated for a generic fighter configuration, and pressure distributions were measured on the chine forebody. All forebody results were obtained in the presence of the wing.

The current authors simulated the flowfield on the Erickson forebody computationally and the results are presented in Ref. 6. For geometries where the crossflow separation location is fixed, the Euler equations were found to produce surface pressure results in good agreement with both the Navier-Stokes equation solutions and the experimental data. Having established the validity of the use of the Euler equations for analysis of chine-shaped forebodies, CFD can then be used for aerodynamic design investigations for this class of shapes, where separated flow is present. Insight into the flowfield physics, which are extremely difficult to obtain experimentally, arise naturally using this approach. The resulting insight provides guidance to aerodynamic designers, and a basis for focusing future experimental investigations on the key portions of the design space.

The purpose of this article is to investigate the effect of various chine-shaped forebody geometries on directional stability characteristics using the approach established in Ref. 6. An analytic forebody that can be used to systematically study forebody aerodynamics for families of forebody shapes at high alpha is proposed. Using this model, a computational study is carried out to determine which shapes lead to the best directional stability characteristics. The results of this computational study are then used to propose some guidelines for high angle-of-attack forebody design.

General Analytic Model: The Generic Forebody

To study geometric shaping effects on forebody aerodynamic characteristics, an analytic forebody model with the ability to produce a wide variation of shapes of interest is defined. This generic forebody model makes use of the equation of a superellipse to obtain the cross-sectional geometry. The superellipse, used previously to control flow expansion around wing leading edges,[7] can recover a circular cross section, as well as produce elliptical and chine-shaped forebody cross sections. Thus, it can be used to define a variety of cross-sectional shapes.

The superellipse equation for the forebody cross section is defined as

$$(z/b)^{2+n} + (y/a)^{2+m} = 1 \tag{1}$$

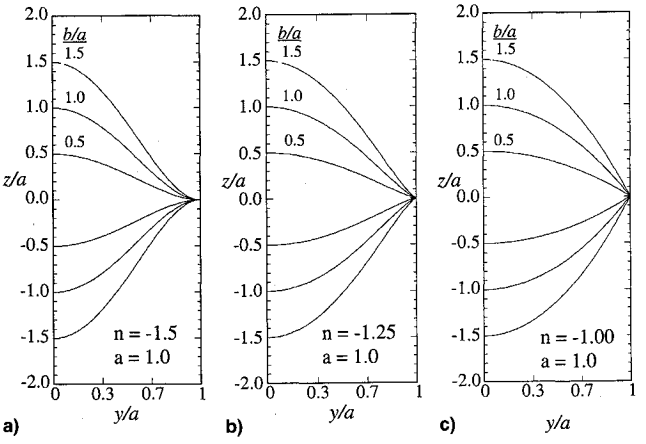

Fig. 2 Cross sections used in the analytic forebody parametric study ($m = 0$): a) $n = -1.5$, b) $n = -1.25$, and c) $n = -1$.

where n and m control the surface slopes at the top and bottom plane of symmetry and chine leading edge. The case $n = m = 0$ corresponds to the standard ellipse. The body is circular when $a = b$.

When $n = -1$, the sidewall is linear at the maximum half-breadth line, forming a distinct crease line. When $n < -1$, the body cross section takes on the cusped or chine-like shape. The derivative of z/b with respect to y/a is

$$\frac{d\bar{z}}{d\bar{y}} = -\frac{[(2 + m)/(2 + n)]}{[1 - \bar{y}^{(2+m)}][(1 + n)/(2 + n)]} \tag{2}$$

where $\bar{z} = z/b$ and $\bar{y} = y/a$. As $\bar{y} \to 1$, (the maximum half-breadth line) the slope becomes

$$\frac{d\bar{z}}{d\bar{y}} = \begin{cases} \infty & n > -1 \\ -(2 + m)\bar{y}^{1+m} & n = -1 \\ 0 & n < -1 \end{cases} \tag{3}$$

The resulting wide variety of cross-sectional shapes is shown in Fig. 2. Different cross sections can be used above and below the maximum half-breadth line to generate asymmetric shapes. More generality can be provided by allowing n and m to be functions of the axial distance x. However, in this study the parameters n and m were taken to be constants with respect to x. The parameters a and b are functions of the axial location x, and can be varied to study planform effects. Notice that when $n = -1$, the value of m can be used to control the slope of the sidewall at the crease line.

Computational Approach

The methodology used for the analytic forebody calculations was similar to that used to compute the flowfield over the Erickson forebody,[6] and builds on the earlier work done on the F-5A[2] and F/A-18.[8] An isolated forebody geometry was used for all the computations presented.

Flowfield Solver

The baseline code for this work was the NASA Langley program CFL3D.[9] The computations were made on the NASA Langley Cray-2S computer. In this code the time-dependent conservation law form of compressible Euler or Reynolds averaged Navier-Stokes equations are solved using a cell-centered finite volume formulation. The code uses a 3-factor implicit time advancement algorithm with multigrid acceleration to the steady-state solution. The Roe-type inviscid flux-difference-splitting scheme option in the code was used to obtain the results presented. Numerous previous investigations have demonstrated the basic capability of the code, e.g., Refs. 2 and 8.

Boundary Conditions

The far-field computational boundaries were chosen sufficiently far away from the body so as not to affect the forces on the body. The forward boundary extends upstream of the nose by $0.57l$, and the radial outer boundary extends $0.97l$ from the model centerline. These values were established after computational experiments on an equivalent tangent-ogive,[10] an F-5A forebody,[10] and work by others on the F/A-18.[8] The reference length l is equal to the longitudinal extent of the forebody which was 30 in.

Freestream values are specified at the far-field boundaries, except along the outflow boundary where a zero-axial-gradient extrapolation condition was used. This extrapolation boundary condition is not strictly valid in subsonic flow, since the wake could affect the flow on the body. To minimize this effect, the computational body length was extended beyond the physical length of the body, keeping the cross section constant. A singularity-type boundary condition was imposed on the boundary that runs from the nose to the far field ahead of it. Flow tangency is enforced on the inviscid body surface. The code was modified slightly to handle the boundary conditions for combined α/β flows. At the plane of geometric symmetry, periodic conditions are used to include sideslip as well as angle of attack in the freestream flow.

Solution Strategy for Parametric Forebody Geometry Study

Based on the analysis of the computational solutions obtained on the Erickson chine forebody,[6] a computational strategy for the forebody shaping study was chosen. It was shown in the case of the Erickson chine forebody that the inviscid predictions were very close to the experimental data. The side force and $C_{n\beta}$ trends were qualitatively similar, and nearly the same for the Euler and turbulent flow computations. Therefore, for chine-shaped geometries where the flow separation location is fixed, Euler computations, which require much less CPU time than turbulent flow computations, can be used to predict the surface pressure distribution.

The computational grids used for this study were generated using a transfinite interpolation grid generator,[11] and were similar to those used in Ref. 6 on the Erickson forebody. A C-O grid topology was used, having 45 points in the radial direction and 101 points in the full circumferential direction. Longitudinally, the grid was clustered near the nose with 25 stations on the forebody as shown in Fig. 3a. A typical cross-sectional grid is shown in Fig. 3b. To avoid large cell volume discontinuities, the surface unit normals were smoothed. This introduced some grid skewness near the chine nose as well as around the chine edge.

The CPU time required for each Euler case on the baseline grid was 3400 s. A grid refinement study was done in Ref. 6 for the Erickson forebody with the inviscid grid. The number of grid points were doubled in the normal direction with increased clustering in the normal direction. The circumferential and axial densities were kept the same. Approximately four fine grid points were packed in the first cell of the baseline grid for the fine inviscid grid. The CPU time required for the fine grid cases were nearly twice those of the baseline grid. Although the grid refinement study made a slight change in the Euler results, it was very expensive considering the minor change in the results. Hence, it was decided that to assess aerodynamic trends arising from forebody geometry variations on chine-shaped forebodies, the computations could be done with the Euler analysis on the baseline grid.

Analytic Chine Forebody Study

Using the generic forebody parametric model defined above, and the computational strategy developed based on the Erickson forebody results,[6] the plan for the investigation of directional stability characteristics of various chine-shaped forebody geometries was developed. It was decided to analyze the effect of changing b/a, n, and combinations thereof. This

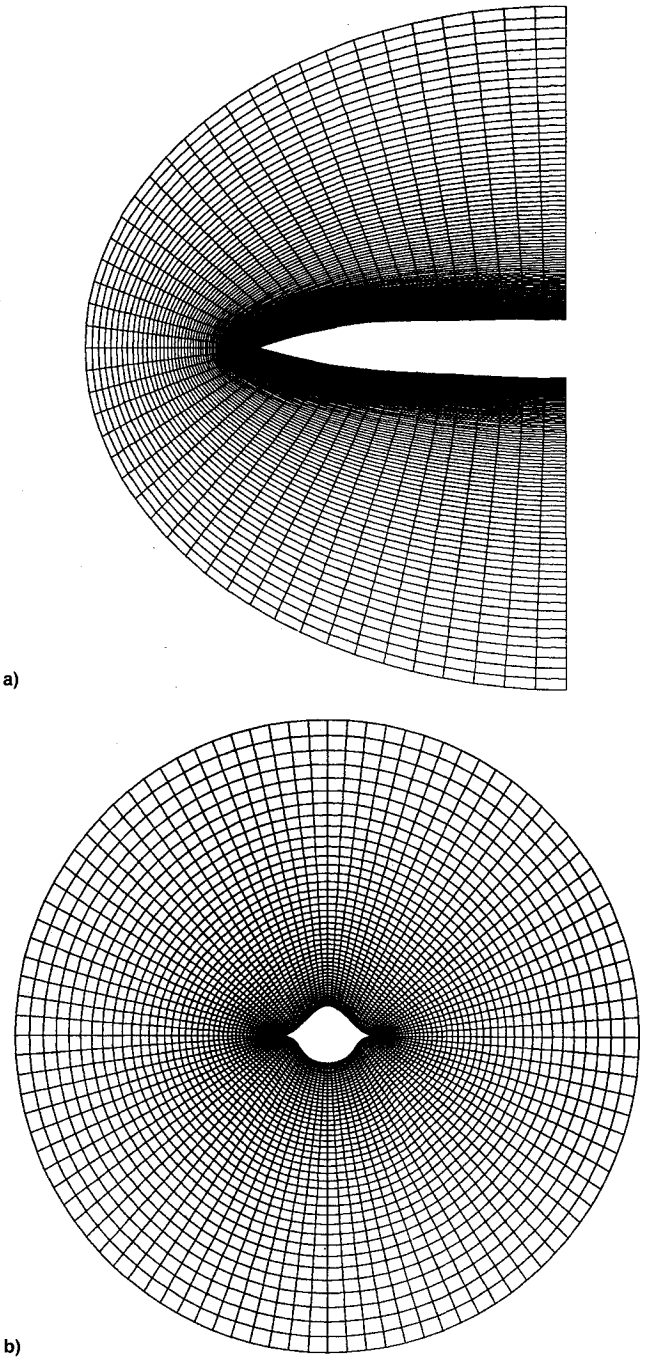

Fig. 3 Inviscid grid used in the analytic forebody geometry: a) longitudinal grid and b) cross-sectional grid at the base plane.

range of cross-sectional shapes provides an extremely broad design space to investigate aerodynamic tailoring of forebody characteristics through geometric design.

Initially, it was decided that the geometric parameters would be $m = 0$, and n would vary between -1 and -1.5 (Fig. 2). The value of b/a was varied between 0.5 and 1.5. The range of flow conditions analyzed was $\alpha = 20 \sim 40$ deg and $\beta = 0 \sim 5$ deg.

The objective of the study was to determine the shape that leads to the highest value of directional stability. This test case matrix resulted in 54 different configurations with symmetrical upper and lower surfaces, and a reduction in study scope was required. The $\beta = 0$-deg cases had been included to compare the flow physics with and without sideslip. However, results at $\beta = 0$ deg produced symmetrical flowfields, $C_n = 0$, and were eliminated. This reduced the number of cases to 27. Further combinations were eliminated as the study progressed and the results examined. However, the study

scope was widened by analyzing some cross sections with asymmetric upper/lower geometries. These geometries were defined using different b/a or different n for upper and lower surfaces.

Initially, the Erickson chine case[5] planform (Fig. 1) was used and the effects of varying cross-sectional geometry were studied. The moment center for the computation of the directional stability was kept fixed at the value used in the Erickson forebody test,[5] which was 12.816 in. from the nose. Based on the best cross-sectional shape, limited planform effects were studied, as presented below.

Results

Effect of Varying b/a

This study was conducted for cross-sectional shapes with $m = 0$, $n = -1.5$, and $b/a = 0.5$, 1, and 1.5 (Fig. 2). Both symmetric and asymmetric upper/lower cross-sectional geometries were analyzed. Figure 4 shows various cross-sectional shapes together with the computed $C_{n\beta}$ for the angle-of-attack range. For symmetrical upper and lower surfaces, the contribution to positive directional stability increases as b/a decreases at a fixed angle of attack. The $b/a = 0.5$ geometry produces the highest $C_{n\beta}$. The Erickson forebody result from Ref. 6 is also included, which is geometrically similar, with symmetrical b/a equal to 0.597. In the asymmetric upper/lower cross-sectional cases, the shallow upper surface ($b/a = 0.5$ upper, $b/a = 1.5$ lower) is seen to provide higher $C_{n\beta}$ than the shallow lower surface geometry. This is because the shallow upper surface ($b/a = 0.5$ upper) results in increased vortex asymmetry compared to $b/a = 1.5$ for the upper surface. Putting the shallow surface on the bottom reduces the negative contribution to side force at any cross section (as shown below). Still, this effect is not as significant as using a shallow upper surface.

Using the $b/a = 0.5$ case as the baseline in Fig. 4, it is interesting to contrast the effects of increasing the body height above and below the chine line. The change of $C_{n\beta}$ with angle of attack differs depending on whether the height is added above or below the chine line. The rate of change of $C_{n\beta}$ with angle of attack is less when thickness is added above the chine line instead of below it. An understanding of these results requires an examination of the flowfield details shown in this study.

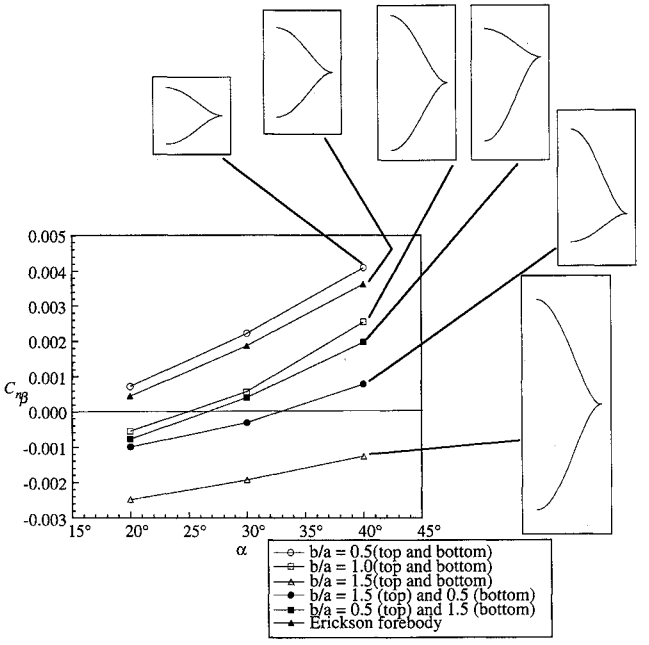

Fig. 4 Effect of varying b/a on the directional stability characteristics, with cross-sectional shapes shown ($\beta = 5$ deg).

Figure 5 shows the variation of the sectional side force with the axial distance for the symmetric b/a geometry cases at $\alpha = 20$ and 40 deg, with the value of β fixed at 5 deg. Near the nose the force is initially destabilizing, being negative for all cases computed. Moving aft from the immediate vicinity of the nose, the trend is reversed and the side force starts to increase toward positive values. The side force becomes more positive with increasing angle of attack. In general, the side force becomes increasingly negative as the value of b/a increases, making the body more unstable. Some crossover occurs at the aft end of the body at the higher α, where the $b/a = 0.5$ case is not as positive as the $b/a = 1$ case.

Figure 6 shows how the side force arises. The difference in pressures on the two sides of the body, ΔC_p, is plotted against the normal coordinate, z, starting at the bottom of the cross section and moving to the top at a typical axial station ($x = 18.35$). The integration of this pressure difference produces the side force value presented in Fig. 5. The cross section below the chine edge always makes a negative contribution to the side force. Above the chine edge there is an abrupt large positive spike in the side force. This arises because of the asymmetry in strength and position of the vortices. At $\alpha = 20$ deg (Fig. 6a), the shallow $b/a = 0.5$ case produces a much larger spike than the $b/a = 1.5$ case. At $\alpha = 40$ deg (Fig. 6b), the $b/a = 1$ case has nearly the same size spike.

The asymmetry in the position and strength of the windward and leeward vortices which is responsible for the positive side force on the forebody is shown in Fig. 7 for $\alpha = 30$ deg and $b/a = 0.5$ and 1.5. Figure 7a presents the minimum static pressure found in the vortex over the length of the body. In this case, the lower pressure for the $b/a = 0.5$ geometry shows that both the leeward and windward vortices are stronger compared to the $b/a = 1.5$ case. Also, the windward vortex for this geometry is much stronger than the leeward vortex resulting in a larger asymmetry. This corresponds to the large

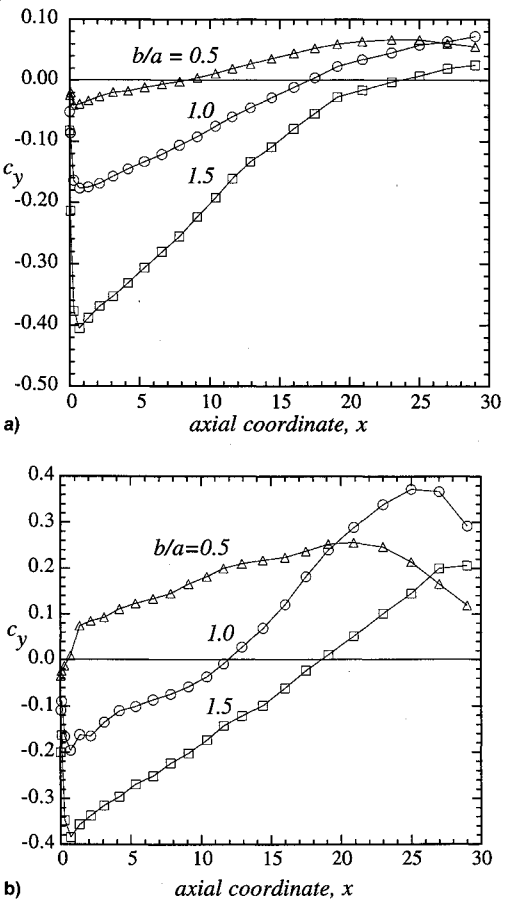

Fig. 5 Effect of varying b/a on sectional side force at different angles of attack: a) $\alpha = 20$ deg, $\beta = 5$ deg and b) $\alpha = 40$ deg, $\beta = 5$ deg.

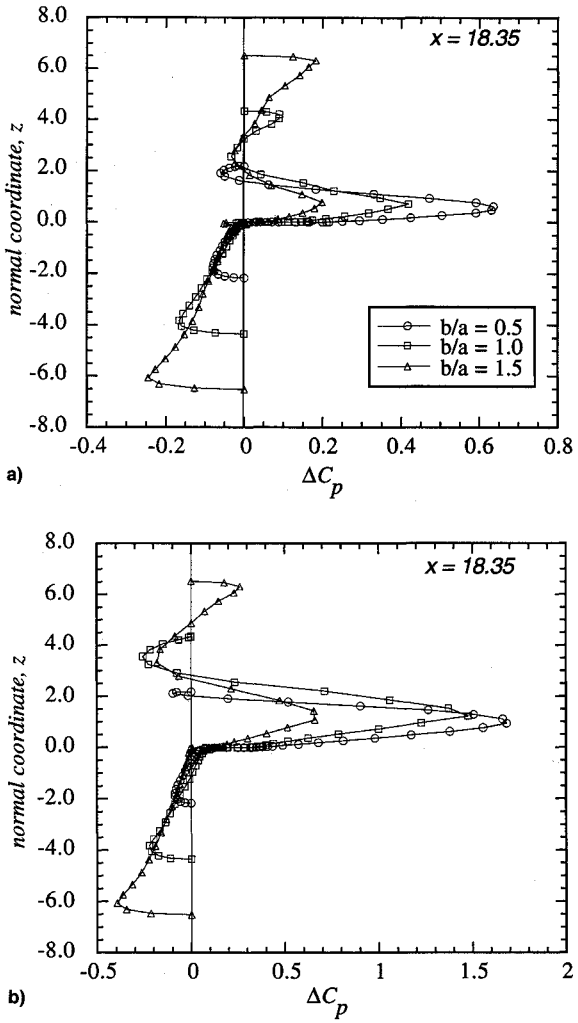

Fig. 6 Effect of varying b/a on ΔC_p: a) α = 20 deg, β = 5 deg and b) α = 40 deg, β = 5 deg.

difference in directional stability shown in Fig. 4. In the sideview shown in Fig. 7b, for b/a = 0.5, both the vortices are further away from the chine line than in the b/a = 1.5 case. The b/a = 0.5 case vortices are above the top centerline, allowing communication between the windward and leeward vortices. In the planform view, Fig. 7c, the b/a = 0.5 case shows more lateral movement, particularly in the aft region, than the b/a = 1.5 case. Here, the windward and leeward vortices are separated by the large hump on the upper surface all along the length of the forebody. This restricts the influence of one vortex on the other, as well as the vortex movement.

Using these results, an understanding of the physics of chined forebody aerodynamics emerges. A shallow upper surface (b/a = 0.5) results in a stronger, more asymmetric vortex system compared to a deep surface (b/a = 1.5). A deep lower surface results in a larger negative contribution to directional stability. Thus, large b/a for either the upper or the lower surface are undesirable.

Effect of Varying Chine Angle

In this study b/a was held constant at 0.5 (corresponding to the best result obtained above), and n was varied over -1.5, -1.25, and -1 (Fig. 2). Recall that, theoretically, the chine edge has a zero angle when $n = -1.5$ and $n = -1.25$, resembling a sharp-edged wing or strake, and therefore has a 180-deg slope discontinuity. When $n = -1$ the included edge angle is finite (127 deg) and the slope discontinuity is smaller.

The effect of changing the shape parameter n on the directional stability is shown in Fig. 8. Essentially, all the results

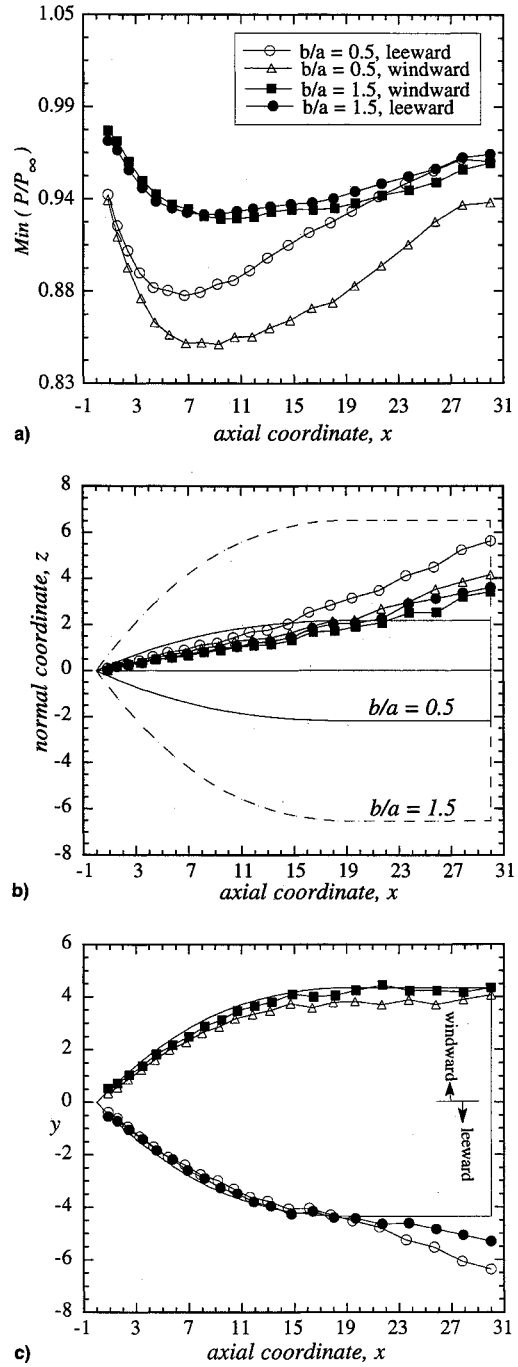

Fig. 7 Vortex strength and position variation with b/a at α = 30 deg and β = 5 deg: a) minimum pressure, b) side view, and c) plan view.

are similar at α = 20 and 30 deg, but show differences at α = 40 deg. The sudden decrease in $C_{n\beta}$ for $n = -1$ at α = 40 deg was further investigated by looking at the side force variation in Fig. 9. Based on the results shown in this figure for the $n = -1$ case over the axial distance from about 3–23, the source of the decrease of $C_{n\beta}$ at α = 40 deg for $n = -1$ can be identified. All the results are similar at α = 20 deg, as expected from Fig. 8. The α = 40-deg case in Fig. 9b provides an indication of how to keep $C_{n\beta}$ from becoming too positive at high angles of attack.

An investigation of the reason for the sudden decrease of $C_{n\beta}$ at α = 40 deg was made. The vorticity being generated due to flow separation has been shown to be proportional to the square of the velocity at the separation point.[12] When $n < -1$ for both upper and lower surfaces, the slope discontinuity is maximum at the chine edge, resulting in large velocities approaching the separation point. Figure 10 shows the

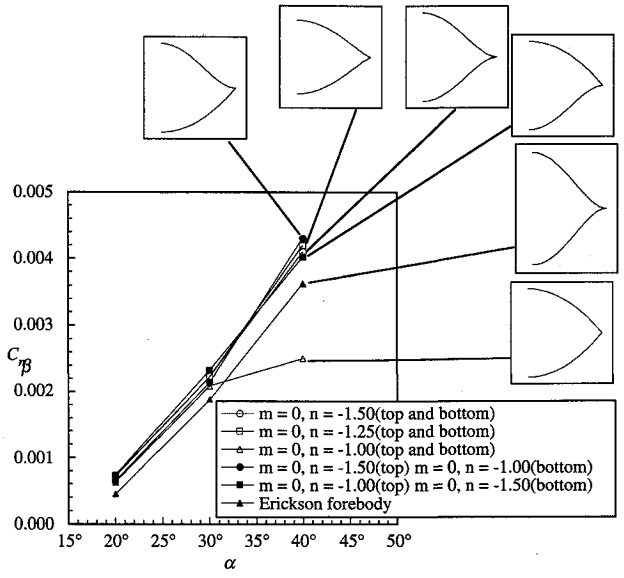

Fig. 8 Variation of directional stability with chine angle (β = 5 deg).

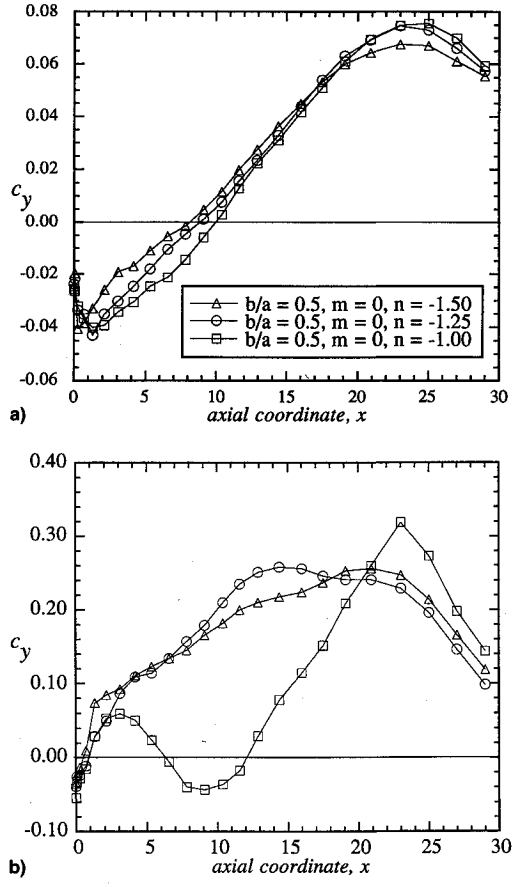

Fig. 9 Variation of sectional side force for different chine angles at different angles of attack: a) α = 20 deg, β = 5 deg and b) α = 40 deg, β = 5 deg.

square of the velocity at the separation point plotted for different chine angles at α = 40 deg. The $n = -1$ case is distinctly different from the other cases. When $n < -1$, very close to the nose the leeward vortex is stronger than the windward vortex, leading to a negative side force. As the axial distance increases the vorticity shed on the windward side increases and the side force is positive. Such observations were also made by Kegelman and Roos[13] based on experimental results. When $n = -1$, as expected, the vorticity shed is much less and of an entirely different character because of reduced slope discontinuity. Moving downstream from the

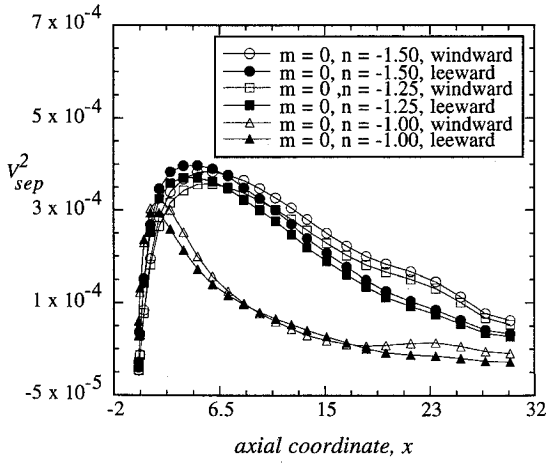

Fig. 10 Comparison of square of velocity at separation point for various chine angles at α = 40 deg and β = 5 deg.

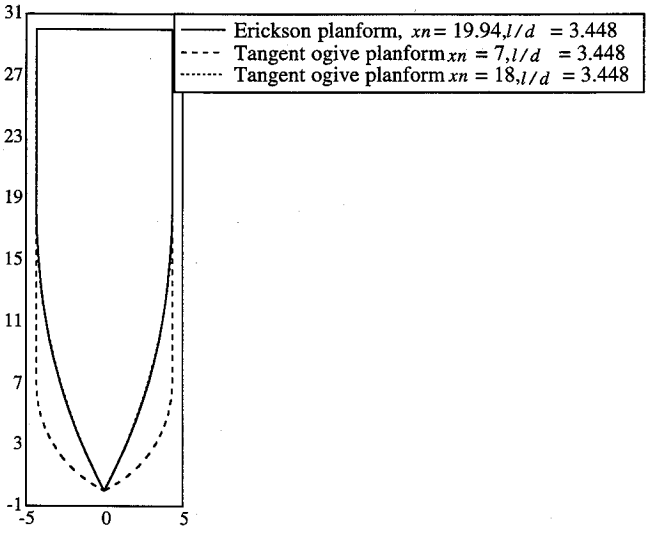

Fig. 11 Planform shapes considered in the present study.

nose, the edge with the largest separation velocity switches sides several times. This is reflected in the side force plot of Fig. 9b. Here, very close to the nose the windward vorticity shed is larger than the leeward vorticity, leading to a positive side force. As we move aft, the side force changes sign as the relative shed vorticity strength changes. This difference in behavior with the different chine angles suggests the existence of a critical angle that controls the rate of feeding of the vortex as the angle of attack changes.

Effect of Varying the Planform Shape

The planform shape for the forebodies studied thus far was the same as that of the Erickson forebody.[6] This planform is shown in Fig. 11. The parameter xn shown for the tangent ogive forebodies is the distance from the tip of the forebody to the station where the planform span becomes a constant. The side force variation in Figs. 5 and 9 showed that most of the positive side force came from the aft portion of the forebody, where the chine line was swept nearly 90 deg. It was thought that expanding to a constant cross section faster would produce a greater positive side force. Because the Erickson planform[6] approximates a tangent ogive with xn = 18, the alternative planform was chosen to be a tangent ogive with xn = 7, as shown in Fig. 11.

The effect of the planform variation on the directional stability is shown in Fig. 12 for three cross-sectional shapes. There is a small increase in $C_{n\beta}$ for a fixed cross-sectional shape with b/a = 0.5, m = 0, and $n = -1$. One other cross section, with a flat lower surface, was computed with this

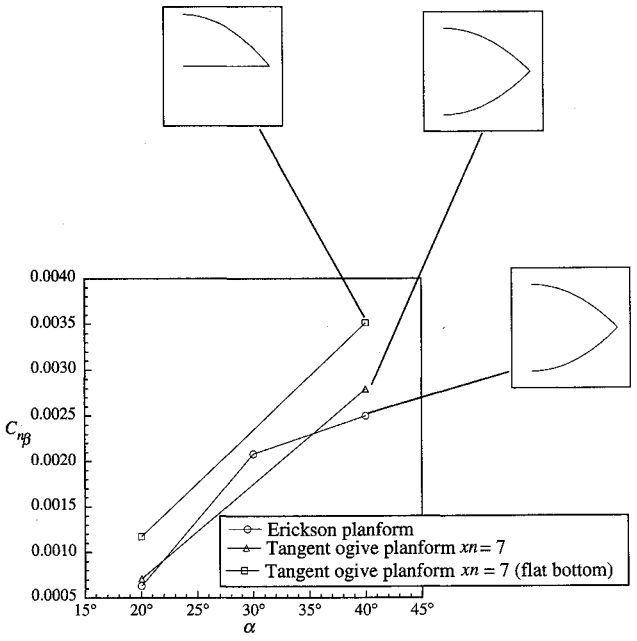

Fig. 12 Effect of planform shape on directional stability characteristics at β = 5 deg (cross-sectional shape defined by m = 0 and n = −1).

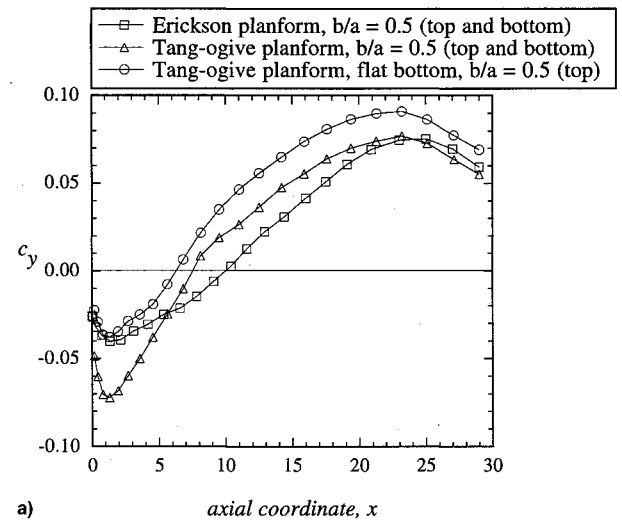

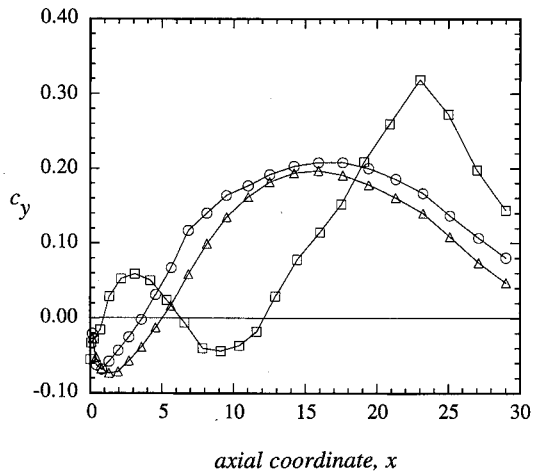

Fig. 13 Effect of planform shapes on variation of sectional side force (cross-sectional shape defined by m = 0 and n = −1): a) α = 20 deg, β = 5 deg and b) α = 40 deg, β = 5 deg.

planform, and resulted in a $C_{n\beta}$ increase. This supported the previous assertion that a smaller b/a on the lower surface reduces the adverse contribution to $C_{n\beta}$ at α = 20 deg, and also at α = 40 deg. Here, note that the chine included angle is much less than the symmetric case. The directional stability continues to increase at α = 40 deg, rather than remain nearly constant, reinforcing the idea that a critical chine angle might exist, which reduces extreme contributions to stability at high angle of attack.

Figure 13 shows the effect of planform shape on side force variation at α = 20 and 40 deg. As expected, after the initial negative side force, the rate of increase of side force is greater in the aft portion of the forebody for the blunt-nosed planform. However, very close to the nose the side force is more negative. Also note, that at α = 40 deg, the double hump is eliminated with a blunt-nosed planform, and with the flat bottom surface the configuration is even better. The connection between planform geometry and shed vortex strength requires further investigation, even in the case of zero sideslip.

Conclusions

For aerodynamic design consideration the following conclusions were made:

1) The best ratio of maximum half-breadth to the maximum centerline width was b/a = 0.5 among the cases analyzed for positive directional stability. In general, lower b/a for both the upper and lower surfaces improves directional stability. In cases where higher b/a is a requirement, it is better to increase the lower surface b/a. This results in a smaller penalty than if we were to increase upper surface b/a. The rate of change of $C_{n\beta}$ with angle of attack is also a function of the surface to which the thickness is added.

2) The effect of chine angle on the directional stability characteristics was found to be insignificant unless the chine angle was large. There could be a critical chine angle beyond which it becomes an important factor. If such a critical angle exists, it provides an indication of how to keep $C_{n\beta}$ from becoming too positive at high angles of attack.

3) The positive contribution to the stability is seen to come from the aft portion of the forebody where the chine line is swept nearly 90 deg. Changing the planform shape by allowing it to expand faster to a constant value, increases the $C_{n\beta}$ only by a small amount. But, the behavior of the side force plots varies significantly for different planform shapes.

Acknowledgments

The results presented were obtained under the support of NASA Langley Research Center through Grant NAG-1-1037. At NASA Langley the technical monitor, Farhad Ghaffari, helped us technically and provided numerous constructive comments. At Virginia Polytechnic Institute and State University, Robert Walters consulted with us regularly on the use of CFL3D. Each of these contributions is gratefully acknowledged.

References

[1]Grafton, S. B., Chambers, J. R., and Coe, P. L., Jr., "Wind-Tunnel Free-Flight Investigation of a Model of a Spin Resistant Fighter Configuration," NASA TN D-7716, June 1974.

[2]Mason, W. H., and Ravi, R., "A Computational Study of the F-5A Forebody Emphasizing Directional Stability," AIAA Paper 91-3289, Sept. 1991.

[3]Chambers, J. R., "High-Angle-of-Attack Aerodynamics: Lessons Learned," AIAA Paper 86-1774, June 1986.

[4]Rom, J., *High Angle of Attack Aerodynamics*, 1st ed., Springer-Verlag, New York, 1992.

[5]Erickson, G. E., and Brandon, J. M., "Low-Speed Experimental Study of the Vortex Flow Effects of a Fighter Forebody Having Unconventional Cross-Section," AIAA Paper 85-1798, June 1985.

[6]Ravi, R., and Mason, W. H., "A Computational Study on Directional Stability of Chine-Shaped Forebodies at High-α," AIAA Paper 92-0030, Jan. 1992.

[7]Mason, W. H., and Miller, D. S., "Controlled Supercritical Cross-flow on Supersonic Wings—An Experimental Verification," AIAA Paper 80-1421, July 1980.

[8]Ghaffari, F., Luckring, J. M., Thomas, J. L., and Bates, B. L., "Navier-Stokes Solutions about the F/A-18 Forebody-LEX Configuration," AIAA Paper 89-0338, Jan. 1989.

[9]Thomas, J. L., Van Leer, B., and Walters, R. W., "Implicit Flux-Split Schemes for the Euler Equations," AIAA Paper 85-1680, July 1985.

[10]Mason, W. H., and Ravi, R., "Hi-Alpha Forebody Design: Part I—Methodology Base and Initial Parametrics," Virginia Polytechnic Inst. and State Univ., VPI-Aero-176, Blacksburg, VA, Oct. 1990.

[11]Ghaffari, F., private communication, NASA Langley Research Center, June 1990.

[12]Mendenhall, M. R., and Lesieutre, D. J., "Prediction of Subsonic Vortex-Shedding from Forebodies with Chines," NASA CR-4323, Sept. 1990.

[13]Kegelman, J. T., and Roos, F. W., "Influence of Forebody Cross-Section Shape on Vortex Flowfield Structure at High Alpha," AIAA Paper 91-3250, Sept. 1991.

MANDATORY — SUBMIT YOUR MANUSCRIPT DISKS

To reduce production costs and proofreading time, all authors of journal papers prepared with a word-processing program are required to submit a computer disk along with their final manuscript. AIAA now has equipment that can convert virtually any disk (3½-, 5¼-, or 8-inch) directly to type, thus avoiding rekeyboarding and subsequent introduction of errors.

Please retain the disk until the review process has been completed and final revisions have been incorporated in your paper. Then send the Associate Editor all of the following:

- Your final version of the double-spaced hard copy.
- Original artwork.
- A copy of the revised disk (with software identified). Retain the original disk.

If your revised paper is accepted for publication, the Associate Editor will send the entire package just described to the AIAA Editorial Department for copy editing and production.

Please note that your paper may be typeset in the traditional manner if problems arise during the conversion. A problem may be caused, for instance, by using a "program within a program" (e.g., special mathematical enhancements to word-processing programs). That potential problem may be avoided if you specifically identify the enhancement and the word-processing program.

The following are examples of easily converted software programs:

- PC or Macintosh TEX and LATEX
- PC or Macintosh Microsoft Word
- PC WordStar Professional
- PC or Macintosh FrameMaker

If you have any questions or need further information on disk conversion, please telephone:

Richard Gaskin
AIAA R&D Manager
202/646-7496

AIAA
American Institute of Aeronautics and Astronautics